



**HAL**  
open science

## Effect of sonication conditions: solvent, time, temperature and reactor type on the preparation of micron sized vermiculite particles

F. Ali, L. Reinert, Jean-Marc Lévêque, L. Duclaux, Fabrice Muller, Shaukat Saeed, Syed Sakhawa Shah

### ► To cite this version:

F. Ali, L. Reinert, Jean-Marc Lévêque, L. Duclaux, Fabrice Muller, et al.. Effect of sonication conditions: solvent, time, temperature and reactor type on the preparation of micron sized vermiculite particles. *Ultrasonics Sonochemistry*, 2014, 21, pp.1002-1009. 10.1016/j.ultsonch.2013.10.010 . insu-00876251

**HAL Id: insu-00876251**

**<https://insu.hal.science/insu-00876251>**

Submitted on 24 Oct 2013

**HAL** is a multi-disciplinary open access archive for the deposit and dissemination of scientific research documents, whether they are published or not. The documents may come from teaching and research institutions in France or abroad, or from public or private research centers.

L'archive ouverte pluridisciplinaire **HAL**, est destinée au dépôt et à la diffusion de documents scientifiques de niveau recherche, publiés ou non, émanant des établissements d'enseignement et de recherche français ou étrangers, des laboratoires publics ou privés.

**Effect of sonication conditions: solvent, time, temperature and reactor type on  
the preparation of micron sized vermiculite particles**

*Farman Ali <sup>a, b, c</sup>, Laurence Reinert <sup>a</sup>, Jean-Marc Leveque <sup>a</sup>, Laurent Duclaux <sup>\*a</sup>, Fabrice Muller<sup>d</sup>, Shaukat Saeed <sup>c</sup>, Syed Sakhawat Shah<sup>b</sup>*

<sup>a</sup> **Laboratoire de Chimie Moléculaire et Environnement, Université de Savoie, 73376 Le Bourget du Lac Cedex, France**

<sup>b</sup> **Department of Chemistry, Hazara University, Mansehra, 21120, Pakistan**

<sup>c</sup> **Department of Metallurgy and Materials Engineering (DMME), Pakistan Institute of Engineering and Applied Sciences (PIEAS), PO Nilore, Islamabad-45650, Pakistan**

<sup>d</sup> **ISTO, 1A Rue de la Férollerie, 42071 Orléans Cedex 2, France.**

\* Corresponding author. Tel.: +33 (0)4 79 75 88 05

E-mail address: [laurent.duclaux@univ-savoie.fr](mailto:laurent.duclaux@univ-savoie.fr)

## **Abstract**

This paper describes the effect of temperature, time, solvent and sonication conditions under air and Argon for the preparation of micron and sub-micron sized vermiculite particles in a Rosett-type reactor. The resulting material were characterized via X-ray powder diffraction (XRDP), Field Emission Scanning Electron Microscopy (FE-SEM), Fourier Transform Infrared (FTIR) Spectroscopy, BET surface area Analysis, chemical analysis (elemental analysis), thermal analysis (TGA) and Laser Granulometry. The sonicated vermiculites displayed modified particle morphologies and reduced sizes (observed by scanning electron microscopy and laser granulometry). Under the conditions used in this work, sub-micron sized particles were obtained after 5 h of sonication, whereas longer times promoted aggregation. Laser granulometry data revealed also that the smallest particles were obtained at high temperature while it is generally accepted that the mechanical effects of ultrasound are optimum at low temperatures. X-ray diffraction results indicated a reduction of the crystallite size along the basal direction (001); but structural changes were not observed. Sonication at different conditions also leads to the surface modification of the vermiculite particles brought out by BET surface measurements and Infrared Spectroscopy. The results indicate clearly that the efficiency of ultrasound irradiation was significantly affected by different parameters such as temperature, solvent, type of gas and reactor type.

**Key words:** Na-Vermiculite, ultrasound, sonication, sub-micron particles, temperature effect, Argon

## 1. Introduction

Vermiculite has been exploited widely over the past 60 years as a valuable insulating, coating, lightweight, high thermal resistivity and filler material among its other uses. It has widespread industrial and agricultural [1] as well as fundamental workability, which can be tailored with the reduction in particle size and or exfoliation [2-3]. Once delaminated and when their particle size and thickness are reduced in a controlled manner, they claim important applications such as absorbents for adsorbing organic contaminants and heavy metals [3– 8], enhancing mechanical and thermal properties of polymeric materials, imparting fire-retardancy and barrier properties for composites [9–11], high temperature and thermal insulating properties [12]. Vermiculite has been proved to be a nice reinforcement for the preparation of nano-composites [3, 13-15]. Vermiculite has a higher surface area to interact with other molecules, as well as a larger interlayer space to enable interaction of organic compounds [3, 16-17]

Different methods have been reported for the delamination and reduction of particle size of vermiculite, such as thermal shock [2-4], mechanical [17-18], sonication [18-24], and chemical treatment with  $H_2O_2$  [25]. Sonication is widely reported method for the delamination of vermiculite, along the [001] lattice direction, to obtain submicron and micron size particles by ultrasonic treatments [19-24]. Ultrasound technology was reported to avoid undesirable side effects such as crystal structure damage of Vermiculite as compared to grinding, because the large range order is almost unaffected by sonication [18, 24, 26].

Cavitation basically involves the formation, growth and collapse of small gas bubble in a liquid exposed to ultrasound irradiation [27-29]. During the cavitational collapse, the temperature and pressure reach thousands of degree of Kelvin and hundreds of atmosphere respectively [27-29].

This physical phenomenon is the cause of several effects, ranging from mechanical to chemical, according to the incident frequency [27-31]. The Physiochemical effects of cavitation are also strongly dependents on the nature of the dissolved gases [31-33] as well as other parameters including the liquid properties, (vapor pressure, viscosity), temperature of sonicated solution and ultrasonic intensity [27-29, 34]. Bubbles of monoatomic gas such as argon, having smaller heat capacity, are known to give much higher temperature upon compression than bubbles of diatomic gases such as ( $O_2$  and  $N_2$ ) [32,]. The solvent used to perform sonication must also be carefully chosen; as solvent viscosity and surface tension are expected to inhibit cavitation: the higher the cohesive forces within a liquid, the more difficult is the cavitation [28, 29]. The temperature of the sonicated solution also plays a vital role. On one hand, high temperatures can help to disrupt solvent-solute interactions, which involve Van der Waals forces, H- bonding and dipole interaction, also faster diffusion occurs at higher temperature. But on the second hand, a too high temperature can also lead to “vaporous” cavitation where acoustic bubbles can do coalescence with natural bubbles of vapor, decreasing the efficiency of the ultrasonic effects [28, 34].

Many references [20-24] reported the particle-size reduction of vermiculite dispersions with high-intensity sonication. They observed reduction of centimetric vermiculite platelets to particles having 15.5  $\mu\text{m}$  average size, after sonication of 10 h in 15 %  $H_2O_2$  [20]. Submicrometric sized particles were obtained (average size of 0.7  $\mu\text{m}$ ) after a sonication period of 80 h [24]. References [21] (or [23]) reported that excess of 40 h (or 100 h) of sonication , yielded to the aggregation of the micrometric particles for which the crystallinity was retained. Nguyen et al. [19] reported also the increase in percentage of the larger micrometric particles after 5 h of sonication in  $H_2O_2$  solution but not in aqueous media. Even if all the above cited

results emphasize the efficiency of ultrasound to decrease the particle size distributions, all reactions times remain important making unreasonable the perspective of a scale-up. In this present work, we decided to study several of the key parameters of the sonication methodology for preparing micron / sub-submicron sized particles of a sodium exchanged vermiculite (Na-VMT). We used an ultrasonic irradiation of 20 kHz in Rosett and cylindrical reactors, and in addition time, temperature, atmosphere conditions and solvent type were explored and optimized. The sonicated vermiculites in various conditions were characterized and compared to raw materials.

## 2. Experimental

### 2.1 Preparation of Na- VMT

Raw vermiculite (Granutec<sup>®</sup> E originating from Yuli China and provided by CMMP, France, named VMT) was first washed with osmosed water to remove the impurities by flotation, dried at 100 °C for 12 h and then milled with a coffee mill to obtain about 0.5 mm basal size particles. The average chemical composition of half a lattice cell calculated from elemental analysis was  $(\text{Si}_{2.87} \text{Al}_{1.07})(\text{Mg}_{2.67} \text{Fe}_{0.29} \text{Ti}_{0.06})\text{O}_{10}(\text{OH})_2\text{K}_{0.48}\text{Na}_{0.22}\text{Ca}_{0.11}$ . A typical procedure for the preparation of Na Vermiculite (Na-VMT) was as follows: 30 g of VMT were submitted to mechanical stirring for 24 hours with 1 mol. L<sup>-1</sup> NaCl (1000 mL) at 25 °C and the solid was separated by sedimentation. The same procedure of cationic exchange was repeated twice. After being exchanged, the Na-VMT was separated by decantation and then washed 10 times with 400 mL of distilled water to remove the excess of sodium and chloride ions and then dried at 100 °C for 24 hours. The average chemical composition of half a lattice cell of the exchanged Na-VMT

calculated from elemental analysis was  $(\text{Si}_{2.87} \text{Al}_{1.07})(\text{Mg}_{2.67} \text{Fe}_{0.29} \text{Ti}_{0.06})\text{O}_{10}(\text{OH})_2\text{K}_{0.40}\text{Na}_{0.49}\text{Ca}_{0.01}$ . The potassium cation was almost not exchanged by sodium but that the calcium ion was nearly totally exchanged.

## 2.2 Sonication

An Ultrasonic Processor (Sonics and Materials, 500 W Ultrasonic Processor - VC505) of 350 W output with a 20 kHz converter fitted with an ultrasonic titanium probe (19 mm- Sonics and Materials, amplitude set to 41 mm) was used. The tip of the horn was dipped into a Rosett double-jacketed (to control the temperature) cell of 60 mL capacity containing Na-VMT suspension prepared in different solvents: osmosed water, hydrogen peroxide (35%  $\text{H}_2\text{O}_2$ ) and toluene. This suspension was sonicated for different periods of time and temperatures. In order to study the effect of reactor geometry, sonication experiments were also carried out in a conventional cylindrical reactor (60 mL capacity) in water.

The calorimetric method was applied to determinate the acoustic power for Rosett and cylindrical reactors. A thermocouple was dipped in the bulk distilled water to record the temperature increase due to sonication (for few minutes). The value of the acoustic power calculated: by the calorimetric method from reference [35], was about 58.7 W for both Rosett and cylindrical reactors. The Rosett type reactor used in this study, revealed in the 80-90's but forgotten since to the best of our knowledge is a reactor with 4 lateral tubes displaying smaller diameters than the body of the reactor. When submitted to the sonic wave, the liquid is pushed in these lateral tubes, leading to a turbulent Venturi effect (rapid acceleration of the liquid). These turbulences allow the formation of hydrodynamic cavitation bubbles whose are then pushed in

the field of the ultrasonic probe. The additional energy brought up by the rapid collapse of these hydrodynamic bubbles might lead to an additional effect with the collapsing acoustic bubbles. In addition, this cell suffered a new modification. The angles and bottom position of the lateral tubes were adapted to optimize the passing of the suspended solution in both the body and the lateral tubes (Fig. 1).

Fig. 1: Modified Rosett-type Reactor.

Typically 5 wt. % of Na-VMT was suspended in  $H_2O$ ,  $H_2O_2$  or toluene (Tolu) under different atmosphere (air or Argon) and submitted to ultrasound for 1 to 8 h to obtain sonicated samples named “S-V- $H_2O$ -T-t”, “S-V- $H_2O_2$ -T-t” and “S-V-Tolu-T-t”, respectively, where T is the temperature of sonication and t is the sonication time. Samples sonicated under Argon in water were referred to “S-V-Argon-T-t”. For all experiments under argon, the vermiculite suspensions were deoxygenized with argon bubbling for 12 h prior to sonication and also during the ultrasonic treatment. A cooling circuit was used to maintain the temperature of the reactor constant during sonolysis at 25 °C, 30 °C, or 90 °C, measured by a thermocouple immersed in the suspension. The percentage of mass of suspended Na-VMT to the total mass of suspension was varied from 2 wt. % to 30 wt. % to study its effect on the particle size reduction.

## **2.3 Characterization**

### **TGA**

The weight loss temperatures of all samples were measured by thermogravimetry (TG) using a Pyris Diamond thermal analyzer (Perkin Elmer, USA). The TG measurements were performed

from room temperature to 1100 °C at a heating rate of 10 °C/min, with a 10 minutes stay at 30 °C under flowing air at a rate of 50 mL/min.

### **Elemental Analysis**

Inductively Coupled Plasma Optical Emission Spectrometry (ICP-OES) analyses of the Na-VMT and some sonicated VMT were performed by continuous wavelength coverage from 167 to 785 nm, using a ICP-OES Thermo Elemental IRIS radial Vista-PRO, at a French accredited laboratory (SARM, CRPG, CNRS, Nancy, France).

### **FTIR**

A Thermo Scientific Nicolet IS10 spectrometer was used for Diffuse Reflectance Infrared Fourier Transform (DRIFT) spectroscopic analysis, using a scanning coverage from 4000 to 400  $\text{cm}^{-1}$  with a spectral resolution of 4  $\text{cm}^{-1}$ , using 64 scans. All samples were kept overnight in an oven, at 80 °C before analysis. Dried potassium bromide (0.54 g), was mixed with vermiculite samples (0.06 g) and grinded to fill the sample holder. A background spectrum of KBr was recorded before each analysis. The DRIFT background-subtracted spectra were commuted to Kubelka Munk units. The infrared spectra were all normalized to their more intense band (*i.e.* the Si-O band in the region of 1000  $\text{cm}^{-1}$ ).

### **XRD**

The crystalline structure of the samples was characterized by X-ray diffraction (XRD) using a Thermo Electron ARL'XTRA diffractometer in Bragg-Brentano ( $\theta$ ,  $\theta$ ) mode goniometer. The device was equipped with a Si (Li) solid detector filtering the  $\text{CuK}\alpha$  radiation ( $\lambda_{\text{CuK}\alpha} =$

1.5418 Å) of a standard European type X-ray tube (40 kV, 40 mA). The divergence, the incident beam scatter, the diffracted beam scatter and the receiving slits were 2.00, 4.00, 0.50 and 0.22 mm wide, respectively. XRD patterns were collected from 1° to 64°.

### **FE-SEM**

To characterize the shape and size of the untreated and sonicated samples SEM analyses were conducted, using a high resolution Field Emission Scanning Electron Microscope [FE-SEM Zeiss Ultra TM55]. A Bruker Silicon Drift EDS Detector coupled with the SEM was used to investigate the chemical nature of the samples

### **BET**

The N<sub>2</sub> adsorption – desorption isotherms were measured using an automatic adsorption instrument (ASAP 2000, Micrometrics) at liquid nitrogen temperature (77 K). Prior to measurements samples were degassed under vacuum (10<sup>-3</sup> mbar) at 100 °C for 12 h . The specific surface area was calculated using the BET (Brunauer – Emmett-Teller) equation by assuming the area of nitrogen molecule to be 0.162 nm<sup>2</sup>.

## **3. Results and discussion**

### **3.1. Chemical compositions**

The main difference in the elemental analysis of the raw samples and the sonicated samples (Table 1) is the increase of the amount of Ti after sonication due to the erosion of the Titanium

probe. Inferred from Table 1, the Ti impurities content in the vermiculites sonicated for 5h in water medium is in the range 0.6-1 weight %.

Recent works [19] have shown that the sonication in H<sub>2</sub>O<sub>2</sub> (35%) of a K-VMT (Table 1), containing Ca<sup>2+</sup>, Na<sup>+</sup>, and mainly K<sup>+</sup> as exchangeable cations (formula : (Si<sub>2.87</sub> Al<sub>1.07</sub>)(Mg<sub>2.67</sub> Fe<sub>0.29</sub> Ti<sub>0.06</sub>)O<sub>10</sub>(OH)<sub>2</sub>K<sub>0.6</sub>Na<sub>0.16</sub>Ca<sub>0.08</sub>), releases preferentially Na<sup>+</sup> in the solution (loss of about 0.7 weight %) rather than K<sup>+</sup>(loss of weight about 0.4 weight %) thanks to the delaminating process induced by cavitation and chemical decomposition of H<sub>2</sub>O<sub>2</sub>. In parallel, the pH of the H<sub>2</sub>O<sub>2</sub> solution increased in order to maintain the electrical neutrality through dissolution of OH<sup>-</sup> anions [4]. This dissolution of the interlayer cations (mainly Na<sup>+</sup>) might affect the chemical composition of the sonicated VMT as the interlayer composition was subsequently modified.

In order to estimate from elemental analysis the half lattice cell chemical formula of the vermiculites (table 1), the excess of Ti content from the probe erosion was subtracted from the whole composition. From the elemental analysis, we have estimated the chemical formula for half a lattice cell of vermiculite material, in the hypothesis that the total charge of the cations belonging to layers was unchanged after sonication. This hypothesis was checked by the comparison of the chemical composition of the layer cations prior and after sonication that gives quite similar contents. However, the loss of hydroxyl anions from the layers was not taking into account for calculating the lattice cell theoretical formula. Computed by this way, the formulas of the two vermiculites sonicated in water at T=25°C or in Argon (i.e. (Si<sub>2.87</sub> Al<sub>1.07</sub>)(Mg<sub>2.67</sub> Fe<sub>0.29</sub> Ti<sub>0.06</sub>)O<sub>10</sub>(OH)<sub>2</sub>K<sub>0.40</sub>Na<sub>0.49</sub>Ca<sub>0.01</sub>), are somewhat very similar to the one of Na-VMT. By contrast the computed formula of the vermiculite sonicated in water at T=90°C shows higher variation of K<sup>+</sup>, Na<sup>+</sup> and Ca<sup>2+</sup> content

(Si<sub>2.87</sub> Al<sub>1.07</sub>)(Mg<sub>2.67</sub> Fe<sub>0.29</sub> Ti<sub>0.06</sub>)O<sub>10</sub>(OH)<sub>2</sub>K<sub>0.48</sub>Na<sub>0.37</sub>Ca<sub>0.03</sub>). Table 1 also shows that among the exchangeable cations, the Na<sup>+</sup> cation remained the more labile as its atomic percentage was decreased after ultrasound irradiation in water, whatever the conditions. The lixiviation of Na<sup>+</sup> cation induced by sonication was improved through rising the solution temperature to 90°C along irradiation.

Table 1: Comparison of the elemental analysis and the atomic % of exchangeable cations of K-VMT and Na-VMT raw and sonicated samples in water and hydrogen peroxide.

### 3.2. TGA

The thermal-gravimetric (TG) analysis curves of Na-VMT and sonicated VMT are presented in Fig. 2. The first weight loss between 40 and 110 °C corresponds to the loss of water physically absorbed on the surface of the clay and in the interlayer spacing brought out by two peaks on the derivative TG signal (not shown)

Concerning this first region (40–110°C), the ultrasonically treated VMT in water (S-V-H<sub>2</sub>O-90 °C- 5h and) showed approximately 5.5 wt. % mass loss and much more than that of the Na-VMT (4.5 %), ascribed to higher hydration of these sonicated samples that might be explained by their higher specific surface areas according to their small sized particles (micron and sub-micron sized particles). By contrast, in the same region of temperature, the sample S-V-H<sub>2</sub>O-25°C-5h displays a lower amount of adsorbed water. As previously reported [25,4] for vermiculites treated by H<sub>2</sub>O<sub>2</sub>, this could be explained by a partial dehydration of the interlayer spacing, due to the insertion-decomposition of hydrogen peroxide in the interlayer spaces. The same dehydration was observed for the vermiculites sonicated at 25 °C for 5h in pure or

deoxygenated water (under argon atmosphere) (samples S-V-Argon-25°C-5h and S-V-H<sub>2</sub>O-25°C-5h) possibly because of the loss some hydrated cations Na<sup>+</sup> released preferentially in the solution after exfoliation instead of K<sup>+</sup> and Ca<sup>2+</sup>, as brought out by the elemental analysis.

The second weight loss from 250 °C to 370 °C, can be attributed to decomposition of some carbonate impurities, present both in sonicated and Na-VMT. The region between 400 and 950 °C records a loss of weight with respect to temperature, which is first attributed to structure water releasing dehydroxylation and then at temperature higher than 850°C to the collapse of the crystal structure octahedral sheet and subsequent transformation around 1000°C in enstatite crystalline phase coexisting with or not with mica-like structure [37] . The emission of water due to the loss of hydroxyl anions from the vermiculite layers occurs at temperature higher than 800 °C for the raw VMT. While TG signal displays almost no change in the range 400-800°C for raw VMT, loss of water is observed continuously in the same range for all the sonicated samples (Fig. 2), as previously reported for ground vermiculite [38]. Moreover the derivative TG signal (not shown) displays a water loss at 525°C in sonicated samples except for S-V-Toluene-25°C-5h. This can be related to the chemical modification (slight removal of the OH<sup>-</sup> anions) due to exfoliation by sonication [4]. The layers might have become less stable with increasing temperature due to the formation of some atomic defects (such as OH<sup>-</sup> vacancies) by irradiation treatments, initiating the dehydroxylation at low temperature. For S-V-H<sub>2</sub>O-25°C-5h sample, the weight increase observed at about 800°C might be attributed to the oxidation of Ti impurities (in TiO<sub>2</sub>) originating from the probe erosion.

Fig. 2: TGA curves of Na-VMT and sonicated vermiculites in different solvents and temperatures.

### 3.3. Infrared Spectroscopy

In comparison to the Na-VMT, sonicated samples exhibit quite similar FTIR spectra (Fig. 3). The large absorption band at  $460\text{ cm}^{-1}$  (Fig. 3) is attributed to the Al-O stretching, while the absorption band at  $680\text{ cm}^{-1}$  is assigned to the Si-O out of plane bending [39]. The main absorption band from  $890\text{ cm}^{-1}$  to  $1100\text{ cm}^{-1}$  represents the asymmetric stretching and bending vibrations of Si-OH network [39]. Silicates generally give two main absorption bands, near  $1000\text{ cm}^{-1}$  (due to Si-O stretching) and near  $600\text{ cm}^{-1}$  (due to Si-O bending). Farmer [40] related the position and intensity of Si-O vibrational bonds, to the delamination of the clay giving oscillation perpendicular to the plates. Similarly Yariv [41, 42] correlated the increase in absorbance and shift to the delamination of kaolinite during the grinding with KBr. FTIR spectra reveal that the main difference with non sonicated raw sample in our case was the behavior of Si-O band, which was shifted to higher wave numbers after sonication treatment (e.g. for S-V-H<sub>2</sub>O-25°C-5h sample, the band is shifted from  $972\text{ cm}^{-1}$  to  $982\text{ cm}^{-1}$ ). Similar shifts were observed for all materials sonicated for same span of time (S-V-H<sub>2</sub>O<sub>2</sub>-25°C-5h, S-V-Argon -25°C-5h, S-V-Toluene-25°C-5h and S-V-H<sub>2</sub>O-90°C-5h). Small shifts in positions ( $\leq 2\text{ cm}^{-1}$ ) of the same band compared to raw Na-VMT were also observed in the infrared spectra recorded for various sonication times (not shown).

Bands at  $3700$ ,  $3666$  and  $3600\text{ cm}^{-1}$  were observed in the OH region . The band at  $3600\text{ cm}^{-1}$  can be attributed to the vibration modes of the inner surface hydroxyl groups, present in the plane shared between the tetrahedral and octahedral sheets [39, 41]. The other two bands are attributed to the coupling of inner surface hydroxyl groups that give a strong Si-OH symmetric stretch at  $3700\text{ cm}^{-1}$  and out of plane vibrations at  $3666\text{ cm}^{-1}$  respectively. The band of OH ( $\delta$ -OH) at  $1641$

$\text{cm}^{-1}$  and  $1636 \text{ cm}^{-1}$  (Figure 3b) are due to the H-O-H adsorbed water bending, previously explained by two kinds of water molecule interacting or not with internal layer cation [43].

Fig. 3: FTIR spectra of Na-VMT and vermiculites sonicated in different solvents and temperatures.

### 3.4. X-Ray Diffraction

Fig. 4 represents the X-ray diffraction patterns of Na-VMT sonicated in different solvents and temperatures. XRD is an effective technique to measure the degree of hydration of Na-VMT. In order to better understand the diffractogram of Na-VMT, we have also prepared two exchanged VMT by Ca (Ca-VMT) and K (K-VMT). The diffractogram of Ca-VMT (not shown) displayed a more intense  $002$  line at  $d_{002}=12 \text{ \AA}$ . The K-exchange of our vermiculite was reported to lead to a complete dehydration and the resulting XRD pattern shows only a single  $002$  line characterized by a basal distance of about  $10 \text{ \AA}$  [19]. In Fig.4 representing the XRD patterns from  $2^\circ$  to  $24^\circ$  ( $2\theta$ ) of the Na-VMT, mainly all the observed peaks correspond to ( $00l$ ) reflections that were attributed to different structures named (a) to (e). The narrow and more intense peak at  $14.97 \text{ \AA}$  (identified as  $002a$ ) corresponds to a layer of homoionic Na VMT with basal distance of  $15 \text{ \AA}$  intercalated with two water layers [44, 45]. The group of ( $002$ ) peaks between between  $13.8$  and  $9.6 \text{ \AA}$  may corresponds to vermiculite layers with lower hydration ratio. The peak at  $10.1 \text{ \AA}$  (identified as  $002e$ ) is attributed to non-hydrated  $\text{K}^+$  homoionic layers resulting from the non-complete exchange of raw VMT with  $\text{Na}^+$ . The peak at about  $12.1 \text{ \AA}$  (identified as  $002c$ ) is attributed to residual  $\text{Ca}^{2+}$  homoionic vermiculite layers (with only one layer of intercalated water) which are much more hydrated than potassic layers but less than Na-

exchanged layers. Peaks at about 12.7 Å (identified as *002b*) and 11.3 Å (*002d*) may correspond to interstratified Na/Ca and Ca/K layers respectively.

A slight broadening of the *001* reflections as well as the disappearance of maxima was observed in all the sonicated material diffractograms (Fig. 4) which might be due to the delamination of vermiculite sheets together with particle size reduction induced by sonication. After sonication, XRD patterns were quite similar, where only broadening of the line and intensity changes were observed, indicating that crystallite structure was not distorted with sonication. Average dimension of the crystallite measured of the sonicated material (along the c-axis) using the Scherrer formula (*002a* at 5.9°) were in the range of 35 to 50 nm compare to 55 nm for the raw Na-VMT. The smallest crystallite sizes were observed in case of sonication for 5h in H<sub>2</sub>O<sub>2</sub> (35 nm) and in H<sub>2</sub>O at 90 °C (40 nm). In all the sonicated samples, whatever the solvent, the *002a* line belonging to the homoionic Na<sup>+</sup> layers was less intense compared to the XRD signal of pristine Na-VMT. This lower intensity can be attributed to the presence of higher amount of less hydrated layers (identified in the second group of *00l* lines referred to *002 b* to *e*) in these sonicated materials. This is in agreement with the chemical analysis (part 3.1) showing a decrease in the Na<sup>+</sup> content after sonication.

Fig 4: Evolution of XRD patterns (normalized to the *010* line) for Na-VMT as well as sonicated Na-VMTs in different solvents and temperature.

### **3.5. Particle Size distribution**

Fig. 5(a) shows the particle size distribution of Na exchanged and sonicated VMTs at various sonication times in aqueous media in the Rosett reactor. Raw Na-VMT exhibited a broad particle size distribution (between 100 and 1000  $\mu\text{m}$ ) where the mean particle size was 100  $\mu\text{m}$ , having a single maxima. Fig. 5a shows an effective decrease in particle size as the sonication time increases. However, beyond 5h of ultrasonic treatment, the particle size distribution increases again. The sample sonicated for 5 h possesses subsequently the smallest particle size (average size in the range 2-8  $\mu\text{m}$ ), where particle sizes below 1  $\mu\text{m}$  were even observed. This might be due to an agglomeration of particles similarly to what was reported in hydrogen peroxide [19, 21]. In addition, Rosett reactor appears to be more efficient for reduction of particle size than the cylindrical reactor because of additional hydrodynamic cavitation (Fig. 5(b)).

Fig. 5(b) compares the distribution of particle size after sonication in different solvents (Toluene,  $\text{H}_2\text{O}_2$  or water using Argon environment) sonicated for a span of 5 h each. Better cavitation phenomenon is observed at lower vapor pressure of the solvent. This is due to the fact that solvents having higher vapor pressure at operating temperature reduce the implosion energy of the bubbles as these are occupied with solvents vapors upon cavitation [28]. Toluene is more volatile than water so that it was less efficient for size reduction. In case of  $\text{H}_2\text{O}_2$ , its high water solubility, low volatility and thermal decomposition is known to lead to the formation of  $\text{O}_2$  and vapor which penetrates into the interlayer leading to the exfoliation of vermiculite [3, 19,25]. It is also known that the sonolytic degradation can lead to the formation of highly reactive and oxidative  $\text{OH}^\circ$  radicals but the production remains rather low at low frequency compared to high frequency [28, 29, 31]. Two modes were observed in the size distribution, whatever the used solvents. After Argon sonication two maxima distribution were observed where particles are distributed between 0.2 and 1  $\mu\text{m}$  and between 1 and 10  $\mu\text{m}$ , respectively, with mechanical

effects of sonication more pronounced in deoxygenated water than in other solvents. In fact, the nature of the gas in the cavitation bubble is known to have a dramatic effect on the cavitation collapse [32]. Some of their properties like solubility, thermal conductivity and heat capacity ratio, affect the sonochemical reaction [28, 32]. Particularly, the  $C_p/C_v$  ratio of the gas in the cavitation bubble affects the temperature produced by the adiabatic compression, and monoatomic gases having high ratio of heat capacity give the highest temperature during the collapsing phase. Similarly the higher the thermal conductivity of the gas, the lower will be the temperature produced during the collapse. According to the hot spot theory [27-29, 32] the sonication should be more energetic under argon due to its lower thermal conductivity. Fig. 5(c) shows the effect of temperature (30 °C or 90 °C) on the particle size distribution through sonication in water, for 3 different span of time, i.e. 1, 3 and 5 h respectively. It is clear that by increasing both the temperature and span of time, particles size is reduced dramatically. In case of S-5-H<sub>2</sub>O-90°C two very sharp distribution modes between 0.1 and 0.3 μm and 1 and 3 μm were observed. This might be attributed to the water vapors going into the interlayer of vermiculite as temperature 90 °C is nearer to the boiling point and yielding to exfoliation. Cavitation bubbles as well as evaporation bubbles might lead to the exfoliation of the clay layers. As vermiculite is a bidimensional material, water evaporation bubbles formed into the lamellar space might promote the exfoliation of clays. Also higher temperature helps in disrupting strong solute matrix interactions and accelerating the diffusion rates.

Fig. 5(d) shows the effect of varying Na-VMT mass (i.e. from 2 to 30 wt. % suspension) in water suspensions against the particle size distribution for 5 h of sonication. For suspension at less than 10 wt. solid % , the size distributions remain very similar

A slight increase in particle size with increasing amount of vermiculite, was found for wt. solid % suspensions higher than 10% explained by the enhanced the suspension viscosity hindering the cavitation effect, but the size variations are in the range 1-3  $\mu\text{m}$  suggesting the interest in scaling-up using 30% suspensions.

Fig. 5: Particle size distributions (percentage of particle volume as a function of particle size): (a) : for various sonication times (sonication in water in Rosett reactor  $T = 25\text{ }^{\circ}\text{C}$ , 5 wt. % Na-VMT in suspension); (b) : for different solvents in rosett reactor (all solvents) and in cylindrical one in case of water solvent. (sonication time = 5h,  $T = 25\text{ }^{\circ}\text{C}$ , 5 wt. % Na-VMT suspension); (c) : as a function of temperature and different span of time (sonication in water, 5 wt. % Na-VMT suspension) ; (d) : for various Na-VMT weight % in suspension (5h sonication in water at  $25^{\circ}\text{C}$ ).

### 3.6. SEM

Several SEM micrographs of the untreated and sonicated Na-VMT are shown in Fig. 6. Fig. 6(a) shows the SEM micrograph of the raw Na-VMT, with a homogenous distribution of platelets having size ranging between 10 to 100  $\mu\text{m}$  as brought out by the laser granulometry characterization. In comparison to Fig. 6(a), all sonicated samples reveal an exfoliated morphology, attributed to the mechanical effect of ultrasound, resulting in the separation of the VMT layers and the formation of submicron size particles. The Fig. 6(b) (*i.e.* S-V- $\text{H}_2\text{O}$ - $25^{\circ}\text{C}$ -5h) reveals size reduction and breaking of the VMT sheets with round edges, and a heterogeneous distribution in terms of particle size which consist of both micron-sized particles and platelets of several tenths of microns size,, in agreement with laser granulometry (Fig. 5c section 3.5). The fig. 6(c) (*i.e.* S-V- $\text{H}_2\text{O}_2$ - $25^{\circ}\text{C}$ -5h) reveals a heterogeneous population, with woolen like structure,

resulting from the intercalation of  $\text{H}_2\text{O}_2$ , followed by the production of molecular oxygen by decomposition, together with the strong mechanical effect of sonication (Fig. 5(b)). In Fig. 6d (S-V- $\text{H}_2\text{O}$ -90°C-5h) particles distribution is heterogeneous, either with population of sub-micron or micron sized particles, in agreement with granulometric repartition (Fig. 5(c) section 3.5). Exfoliated VMT platelets of very thin size, few in number, very well separated from each other and even flakes with curved morphology can be clearly observed, which could be attributed to the highest degree of exfoliation achieved due to the sonication at high temperature. Indeed, at high temperature cavitation bubbles together with the boiling vapors result in an extraordinary exfoliation, as previously described (section 3.5). The lengths of the smallest exfoliated VMT flakes measured directly from the SEM micrographs are  $\sim 170$  nm. This result indicates that high temperature based sonication produced finest particle sizes together with high exfoliated morphology as compared to other systems. These observations are consistent with the laser granulometry results.

Fig. 6(e) reveals the SEM micrograph of S-V-Toluene-25°C-5; in which are observed round shape agglomerates of small particles with an irregular symmetry resulting from the fracture of the vermiculite layers. In case of toluene, only slight exfoliation was observed, in the absence of chemical exfoliation and intercalation of toluene, so that very thick sheets were obtained compared to other solvent. S-V-Argon-25°C SEM image (Figure 6(f)) includes again an heterogeneous distribution, as in accordance with the granulometry data, formed of dense particles, which seems to be due to colonization of the smaller particles. This could be attributed to the effectiveness of sonication under monoatomic gases, as previously discussed (part 3.6) giving  $\sim 345$  nm length flakes.

Fig. 6: Scanning Electron Micrographs of (a) Na- VMT, (b) S-V-H<sub>2</sub>O at 25°C, (c) S-V-H<sub>2</sub>O at 90°C, (d) S-V-H<sub>2</sub>O/Argon at 25°C (e) S-V-H<sub>2</sub>O<sub>2</sub> at 25°C and (f) S-V-Toluene at 25°C

### 3.6. BET Specific surface Area

Table 2 shows the BET specific surface areas for all VMT samples for different spans of time in different solvents and temperature. The sonication leads to a gradual increase in specific surface area as after 1 h of sonication the surface area increases from 3.6 m<sup>2</sup>/g to 15.4 m<sup>2</sup>/g, and keep on increasing until 8h of sonication reaching 34.3 m<sup>2</sup>/g. Also; the nature of the solvent on the specific surface area and particle size was confirmed. In comparison to toluene, H<sub>2</sub>O<sub>2</sub> and H<sub>2</sub>O solvents are better giving the highest surface area for the same conditions of sonication (time, temperature and power). S-V-H<sub>2</sub>O-90°C-5h sample presents the highest BET specific surface area for particles prepared for the same irradiation time, in agreement with its highly exfoliated aspect observed by SEM (Fig. 6-c) and its smallest particle size brought out using laser granulometry.

Table 2: BET specific surface area measured as a function of sonication time and temperature

### Conclusion

This study has shown the effectiveness of the rosett reactor for the preparation of micron sized Na-VMT particles by sonication at 20 KHz. Laser Granulometry distribution reveals in sonicated Na-VMT suspensions, the presence of two modes of particle size, one with average micron sized particles and another in the sub-micron range. Particle size analysis establishes the effectiveness of sonication for particle size reduction explained by mechanical shock of cavitation bubble

implosion. The sonication promoted also the preferential dissolution of the  $\text{Na}^+$  exchangeable cations due to the delamination and further separation of the clay mineral layers. The delamination was monitored by the choice of the sonication conditions: solvent nature, and temperature.

XRD results of the sonicated Na-VMT show only slight broadening of the *001* reflection was. The average crystallite size measured using Scherrer formula was in the range of 35 to 50 nm. FT-IR spectra reveal that the Si-O bond is shifted to higher wave number, after sonication treatment. The time length of 5 h sonication was found to give in water media, the reduced particle size, beyond which an increase in particle size was observed due to reagglomeration. The sonication in water yielded to mainly micrometric particles.

The use of deoxygenated water using argon has improved the cavitation as samples sonicated under this monoatomic gas recorded a size distribution with important submicrometric additional mode between 0.2 to 1  $\mu\text{m}$  and 1  $\mu\text{m}$  to 10  $\mu\text{m}$ , emphasizing that the mechanical effect was more pronounced here as compare to other solvent.

The most striking effect was observed for sonication at higher temperature, as particle size was dramatically reduced by increasing the temperature and span of time. In this case, the distribution mode between 0.1  $\mu\text{m}$  and 0.3  $\mu\text{m}$  is more intense compared to second micrometric mode (1  $\mu\text{m}$  to 3  $\mu\text{m}$ ). This could be attributed to the improved exfoliation and delamination brought about by cavitation as well as natural evaporation bubbles of the chosen solvents at this temperature.

SEM reveals a more or less exfoliated morphology, with heterogeneous distribution in terms of particle size for all sonicated samples (exfoliated flake average  $\sim 170$  nm), showing the effectiveness of ultrasound. For samples sonicated at  $90^\circ\text{C}$  in water, SEM observed VMT platelets were especially exfoliated with very thin size. Thus, the efficiency of sonication at  $90^\circ\text{C}$

in water yield to improved exfoliation, attributed to the effect of boiling vapors accompanying cavitation bubbles at this temperature.

## **Acknowledgment**

This work was supported by the HEC & FRENCH Embassy in Pakistan (SCAC), under a JOINT SPLIT PH.D FELLOWSHIP (Sandwich) Program.

## References:

- [1] J. Konta, Clay and man: clay raw material in the service of man, *Appl. Clay Sci.* 10 (1995) 275-335.
- [2] Hindman J.R. Vermiculite, in: D.D. Carr (Eds.), *Industrial minerals and rocks* 6th edition, Society for Mining Metallurgy and Exploration Inc., Littleton, Colorado, 1994, pp. 1103–1111.
- [3] M. Valaškova, G. Simha Martynkova, Vermiculite: structural properties and examples of the use, in: M. Valaškova, G. Simha Martynkova (Eds.), *Clay minerals in nature - their characterization, modification and application*, InTech, pp. 209-238. (DOI: 10.5772/2708)
- [4] M. Kehal, L. Reinert, D. Maurin, J.L. Bantignies, F. Ohashi, A. Mennour, L. Duclaux, The trapping of boron from water by exfoliated and functionalized vermiculite, *Clay. Clay Miner.* 56 (4) (2008) 453-460.
- [5] M. Kehal, L. Reinert, L. Duclaux, Characterization and boron adsorption capacity of vermiculite modified by thermal shock or H<sub>2</sub>O<sub>2</sub> reaction and/or sonication, *Appl. Clay Sci.* 48 (2010) 561-568.
- [6] M.F. Brigatti, T.A. Laurora, D. Malferrari, L. Medici, L. Poppi, Adsorption of [Al(Urea)<sub>6</sub>]<sup>3+</sup> and [Cr(Urea)<sub>6</sub>]<sup>3+</sup> complexes in the vermiculite interlayer, *Appl. Clay Sci.* 30 (2005) 21-32.
- [7] D. Malferrari, M.F. Brigatti, A. Laurora, S. Pini, L. Medici, Sorption kinetics and chemical forms of Cd(II) sorbed by thiol-functionalized 2:1 clay minerals, *J. Hazard. Mater.* 143 (2007) 73-81.

- [8] A.C. Vieira Dos Santos, J.C. Masini, Evaluating the removal of Cd(II), Pb(II) and Cu(II) from a waste water sample of a coating industry by adsorption onto vermiculite, *Appl. Clay Sci.* 1-2(37) (2007) 167–174.
- [9] S.J. Ahmadi, Y.D. Huang, W. Li, Synthetic routes, properties and future applications of polymer-layered silicate nanocomposites, *J. Mater. Sci.* 39 (2004) 1919-1925.
- [10] S.S. Ray, M. Bousmina, Biodegradable polymers and their layered silicate nanocomposites: in greening the 21st century materials world, *Prog. Mater. Sci.* 50 (2005) 962-1079.
- [11] S. Takahashi, H.A. Goldberg, C.A. Feeney, D.P. Karim, M. Farrell, K. O'Leary, D.R. Paul, Gas barrier properties of butyl rubber/vermiculite nanocomposite coatings, *Polym.* 47 (2006) 3083-3093.
- [12] M.J. Potter, Vermiculite: U.S. Geological Survey Minerals Year book, 2003, pp. 81.1-81.3.
- [13] K. Zhang, J. Xu, K.Y. Wang, L. Cheng, J. Wang, B. Liu, Preparation and characterization of chitosan nanocomposites with vermiculite of different modification, *Polym. Degd. Stab.* 94 (2009) 2121-2127.
- [14] C. Yang, P. Liu, J. Guo, W. Yang, Polypyrrole/vermiculite nanocomposites via self-assembling and in situ chemical oxidative polymerization, *Synth. Metal.* 160 (2010) 592-598.
- [15] T. Zhaobin, L. Peng, G. Jinshan and S. Zhixing, Preparation of polyaniline/vermiculite clay nanocomposites by in situ chemical oxidative grafting polymerization, *Polym. Int.* 58 (2009) 552-556.

- [16] L. Wang, Z. Chen, X. Wang, S. Yan, J. Wang, Y. Fan, Preparations of organo-vermiculite with large interlayer space by hot solution and ball milling methods: A comparative study, *Appl. Clay Sci.* 51 (2011) 151-157.
- [17] D.G. H. Ballard, G. R. Rideal, Flexible inorganic films and coating, *J. Mat. Sci.* 18 (1983) 545-561.
- [18] L.A. Pérez-Maqueda, M.C. Jiménez de Haro, J. Poyato, J.L. Pérez-Rodríguez, Comparative study of ground and sonicated vermiculite, *J. Mat. Sci.* 39 (2004) 5347-5351.
- [19] A.N. Nguyen, M. Kehal, L. Reinert, J.M. Leveque, A. Beziat, P. Dehaut, J.F. Juliaa L. Duclaux, Preparation and characterization of micron and submicron-sized vermiculite powder by ultrasonic irradiation, *Appl. Clay Sci.* 72 (2013) 9-17.
- [20] L.A. Perez-Maqueda, O.B. Caneo, J. Poyato, J.L. Perez-Rodriguez, Preparation and characterization of micron and submicron-sized vermiculite, *Phys. Chem. Miner.* 28 (2001) 61-66.
- [21] A. Wiewiora, J.L. Perez-Rodriguez, J.L. Perez-Maqueda, J. Drapala, Particle size distribution in sonicated high- and low- charge vermiculites, *Appl. Clay Sci.* 24 (2003) 51-58.
- [22] M.C. Jimenez de Haro, J.M. Martinez Blanes, J. Poyato, L.A. Pérez-Maqueda, A. Lerf, J.L. Pérez-Rodríguez, Effect of mechanical treatment and exchanged cation on the micro porosity of vermiculite, *J. Phys. Chem. Solid.* 65, (2004) 435-439.
- [23] J. Poyato, J.L. Perez-Rodriguez, V. Ramirez-Valle, A. Lerf, F.E. Wagner, sonication induced redox reaction of the Ojen (Andalucia, Spain) vermiculite, *Ultrason. Sonochem.* 16 (2009) 570-576.

- [24] J. L. Perez-Rodriguez, F. Carrera, J. Poyato, L. A. Perez-Maqueda, Sonication as a tool for preparing nanometric vermiculite particles, *Nanotech.* 13 (2002) 382-387.
- [25] V.A. Muromtsev, N.M. Zolotukhina, A.K. Mamina, X-ray, IR spectroscopic, and Chemical analysis of products of reaction between vermiculite and hydrogen peroxide, *Inorg. Mater.* 26 (1990) 868-871.
- [26] L.A. Perez-Maqueda, A. Duran, J.L. Perez-Rodriguez, Preparation of submicron talc particles by sonication, *Appl. Clay Sci.* 28 (2005) 245-255.
- [27] M.M. Van Iersel, *Sensible Sonochemistry*, PhD thesis, Technical University of Eindhoven, Netherlands, 2008.
- [28] T.J. Mason, *Practical Sonochemistry: User's Guide to Applications in Chemistry and Chemical Engineering*, Ellis Horwood Ltd, New York, 1992.
- [29] H.M. Santos, C. Lodeiro, J.L. Capello-Martinez, the Power of Ultrasound, in: J.L. Capello-Martinez (Eds.), *Ultrasound in Chemistry: Analytical Applications*, Wiley - Vch Verlag GmbH & Co. KGaA, Weinheim, 2009, pp. 1–15.
- [30] S.J. Doktycz, K.S. Suslick, Interparticle collisions driven by ultrasound, *Science* 247, (1990) 1067-1069.
- [31] M. H. Entezari, P. Kruus, R. Otson, The effect of frequency on sonochemical reactions III: dissociation of carbon disulfide, *Ultrason. Sonochem.* 4 (1997) 49-54.
- [32] J. Rooze, E.V. Rebrov, J.C. Schouten, J.T.F. Keurentjes, Dissolved gas and ultrasonic cavitation – A review, *Ultrason. Sonochem.* 20 (2013) 1–11.
- [33] R. Ogawa, K. Takashi, H. Hidemi, Q.L. Zhao, S. Fukuada, P. Riesz, Effects of dissolved gases and an echo contrast agent on ultrasound mediated in vitro gene transfection, *Ultrason. Sonochem.* 9 (2002) 197-203.

- [34] B. Niemczewski, Observations of water cavitation intensity under practical ultrasonic cleaning conditions, *Ultrason. Sonochem.* 14 (2007) 13-18.
- [35] R.F. Contamine, A.M. Willhelm, J. Berlan, H. Delmas, Power measurement in sonochemistry, *Ultrason. Sonochem.* 2 (1995) S43-S47.
- [36] G.F. Walker, W.F. Cole, The vermiculite minerals. In: Mackenzie, R.C. (Ed.), the Differential Thermal Investigation of Clays. Mineralogical Society, London, 1957 pp.191-207.
- [37] C. Marcos, Y.C. Arango, I. Rodriguez, X-ray diffraction studies of the thermal behaviour of commercial vermiculites, *Appl. Clay Sci.*42 (2009) 368–378.
- [38] V. Balek, J. L. Pérez-Rodríguez, L. A. Pérez-Maqueda, J. Šubrt, J. Poyato, J. Therm. Anal. and Calorim. 88 (2007) 819–823.
- [39] V.C. Farmer, the Infrared Spectra of Minerals. Mineralogical Society, London, 1974.
- [40] V. C. Farmer, Invited review Infrared Spectroscopy in clay mineral studies *Clay Minerals Macaulay Institute or Soil Research, Aberdeen*, 7, 1968 pp. 373-387.
- [41] S. Yariv, Some effects of grinding kaolinite with potassium bromide, *Clays Clay Miner.* 23 (1975) 80-82.
- [42] S. Shoval, S. Yariv, K. H. Michaelian, M. Boudeulian, G. Panczer, Hydroxyl-stretching Raman and infrared bands 'A' and 'Z' in spectra of kaolinites, *Clay Miner.* 34 (1999) 551-563.
- [43] G. Sposito, R. Prost, Structure of water adsorbed on smectites, *Chem. Rev.* 826(1982) 553-573.
- [44] L.A. Pérez-Maqueda, V. Balek, J. Poyato, J.L. Pérez-Rodríguez, J. Šubrt, I.M. Bountsewa, I.N. Beckman, Z. Málek, Study of natural and ion exchanged vermiculite

by emanation thermal analysis, TG, DTA and XRD, *J. Thermal Anal. Cal.* 71 (2003) 715–726.

- [45] F.H. Muiambo, W.W. Focke, M. Atanasova, I. van der Westhuizen, L.R. Tiedt, Thermal properties of sodium-exchanged palabora vermiculite, *Appl. Clay Sci.* 50 (2010) 51–57.

## Figure Captions

Fig. 1: Modified Rosett-type Reactor.

Fig. 2: TGA curves of Na-VMT and sonicated vermiculites in different solvents and temperatures.

Fig. 3: FTIR spectra of Na-VMT and vermiculites sonicated in different solvents and temperatures.

Fig 4: Evolution of XRD patterns (normalized to the *010* line) for Na-VMT as well as sonicated Na-VMTs in different solvents and temperature.

Fig. 5: Particle size distributions (percentage of particle volume as a function of particle size): (a) : for various sonication times (sonication in water in Rosett reactor  $T = 25\text{ }^{\circ}\text{C}$ , 5 wt. % Na-VMT in suspension); (b) : for different solvents in rosett reactor (all solvents) and in cylindrical one in case of water solvent. (sonication time = 5h,  $T = 25\text{ }^{\circ}\text{C}$ , 5 wt. % Na-VMT suspension); (c) : as a function of temperature and different span of time (sonication in water, 5 wt. % Na-VMT suspension) ; (d) : for various Na-VMT weight % in suspension (5h sonication in water at  $25^{\circ}\text{C}$ ).

Fig. 6: Scanning Electron Micrographs of (a) Na- VMT, (b) S-V- $\text{H}_2\text{O}$  at  $25^{\circ}\text{C}$ , (c) S-V- $\text{H}_2\text{O}$  at  $90^{\circ}\text{C}$ , (d) S-V- $\text{H}_2\text{O}$ /Argon at  $25^{\circ}\text{C}$  (e) S-V- $\text{H}_2\text{O}_2$  at  $25^{\circ}\text{C}$  and (f) S-V-Toluene at  $25^{\circ}\text{C}$ .



Fig. 1: Modified Rosett-type Reactor.

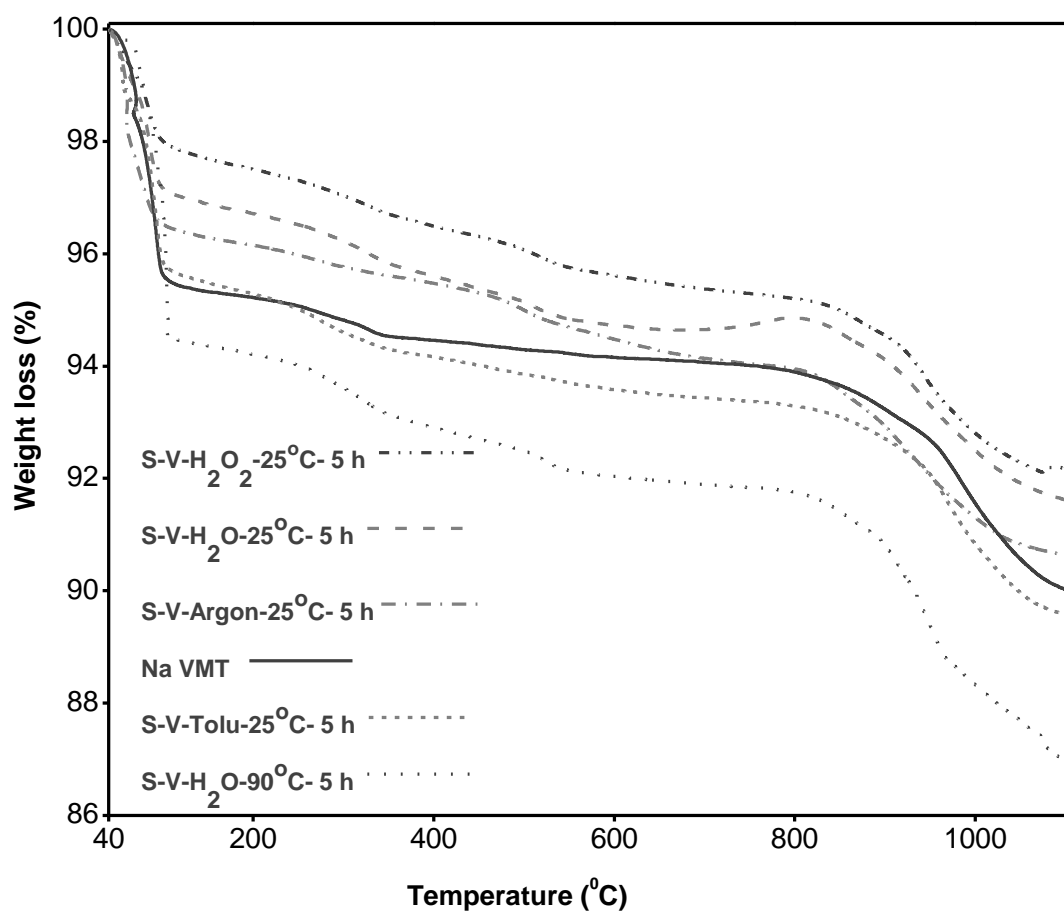


Fig. 2: TGA curves of Na-VMT and sonicated vermiculites in different solvents and temperatures.

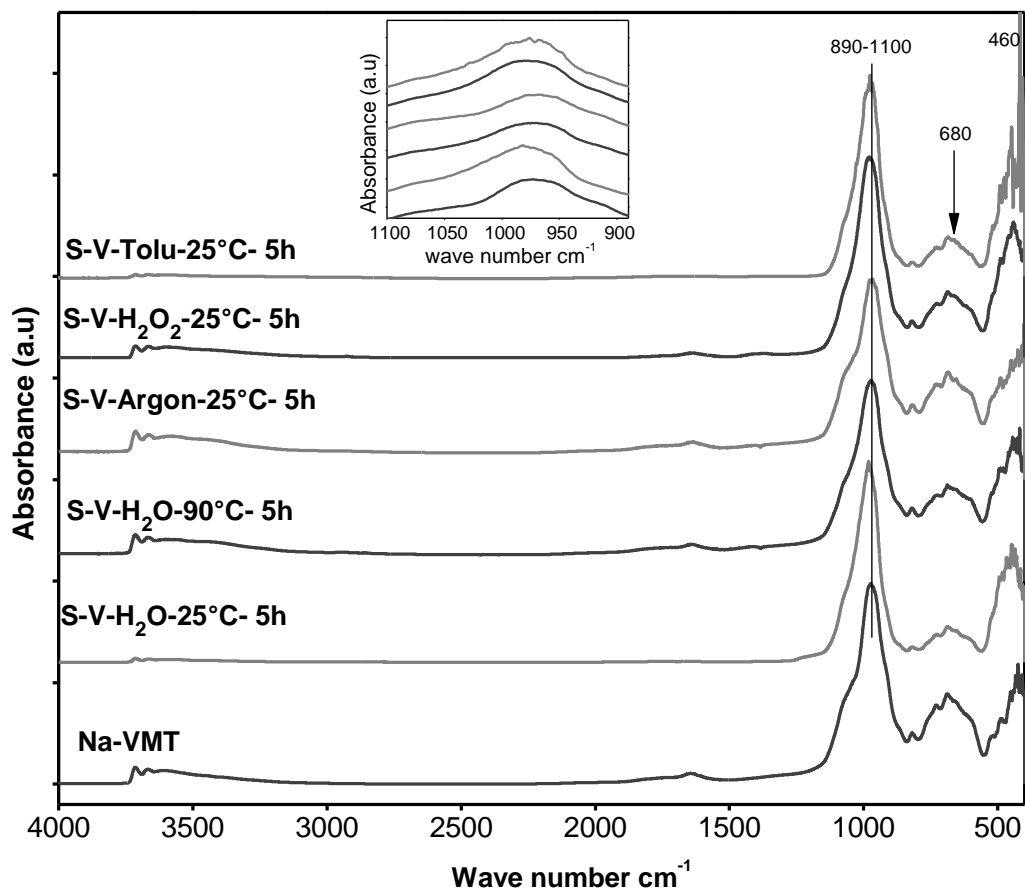


Fig. 3: FTIR spectra of Na-VMT and vermiculites sonicated in different solvents and temperatures.

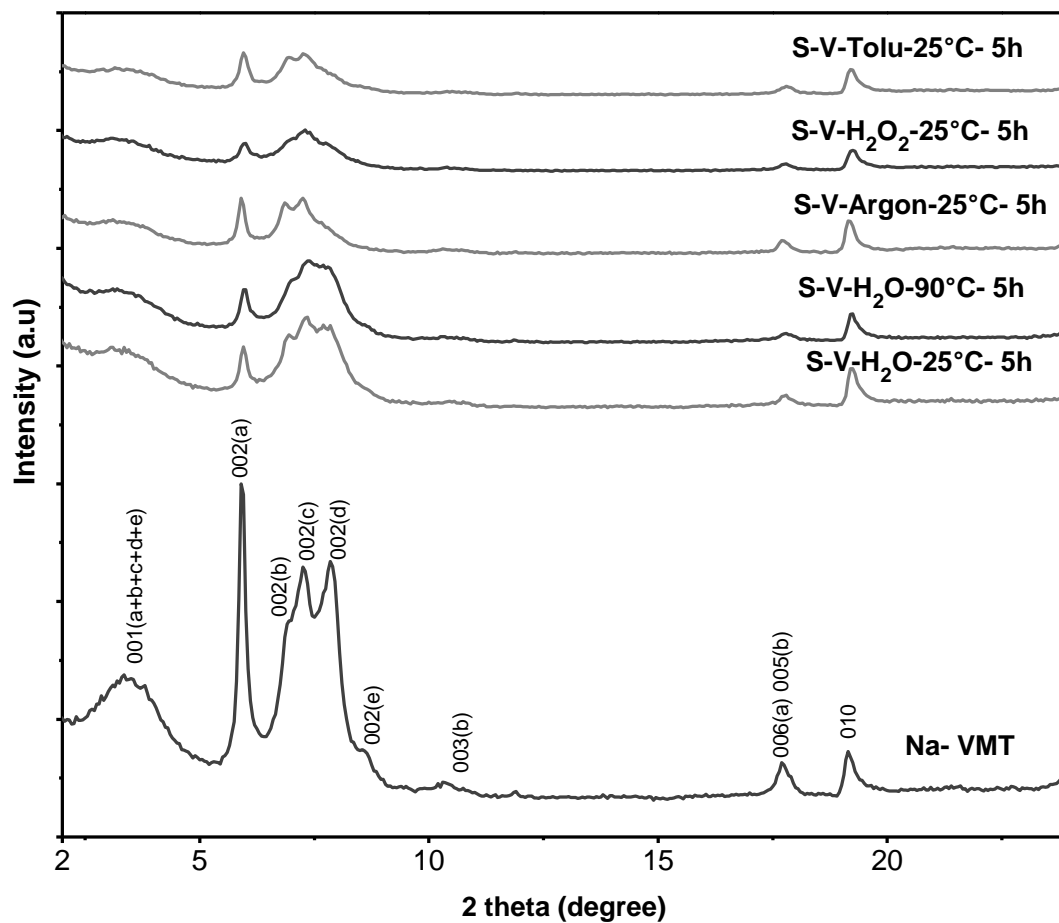


Fig 4: Evolution of XRD patterns (normalized to the 010 line) for Na-VMT as well as sonicated Na-VMTs in different solvents and temperature.

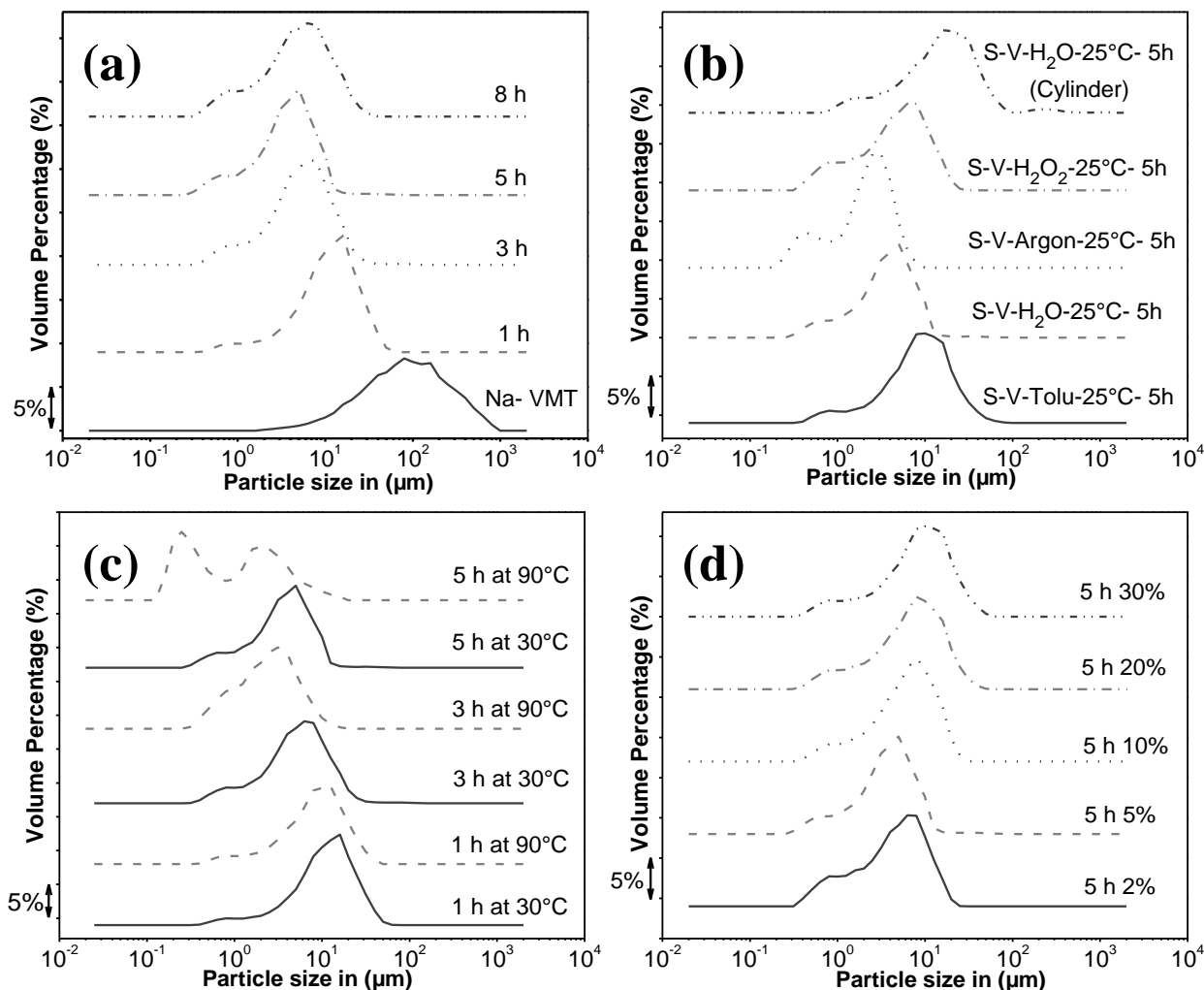


Fig. 5: Particle size distributions (percentage of particle volume as a function of particle size): (a) : for various sonication times (sonication in water in Rosett reactor  $T = 25\text{ }^{\circ}\text{C}$ , 5 wt. % Na-VMT in suspension); (b) : for different solvents in rosett reactor (all solvents) and in cylindrical one in case of water solvent. (sonication time = 5h,  $T = 25\text{ }^{\circ}\text{C}$ , 5 wt. % Na-VMT suspension); (c) : as a function of temperature and different span of time (sonication in water, 5 wt. % Na-VMT suspension) ; (d) : for various Na-VMT weight % in suspension (5h sonication in water at  $25\text{ }^{\circ}\text{C}$ ).

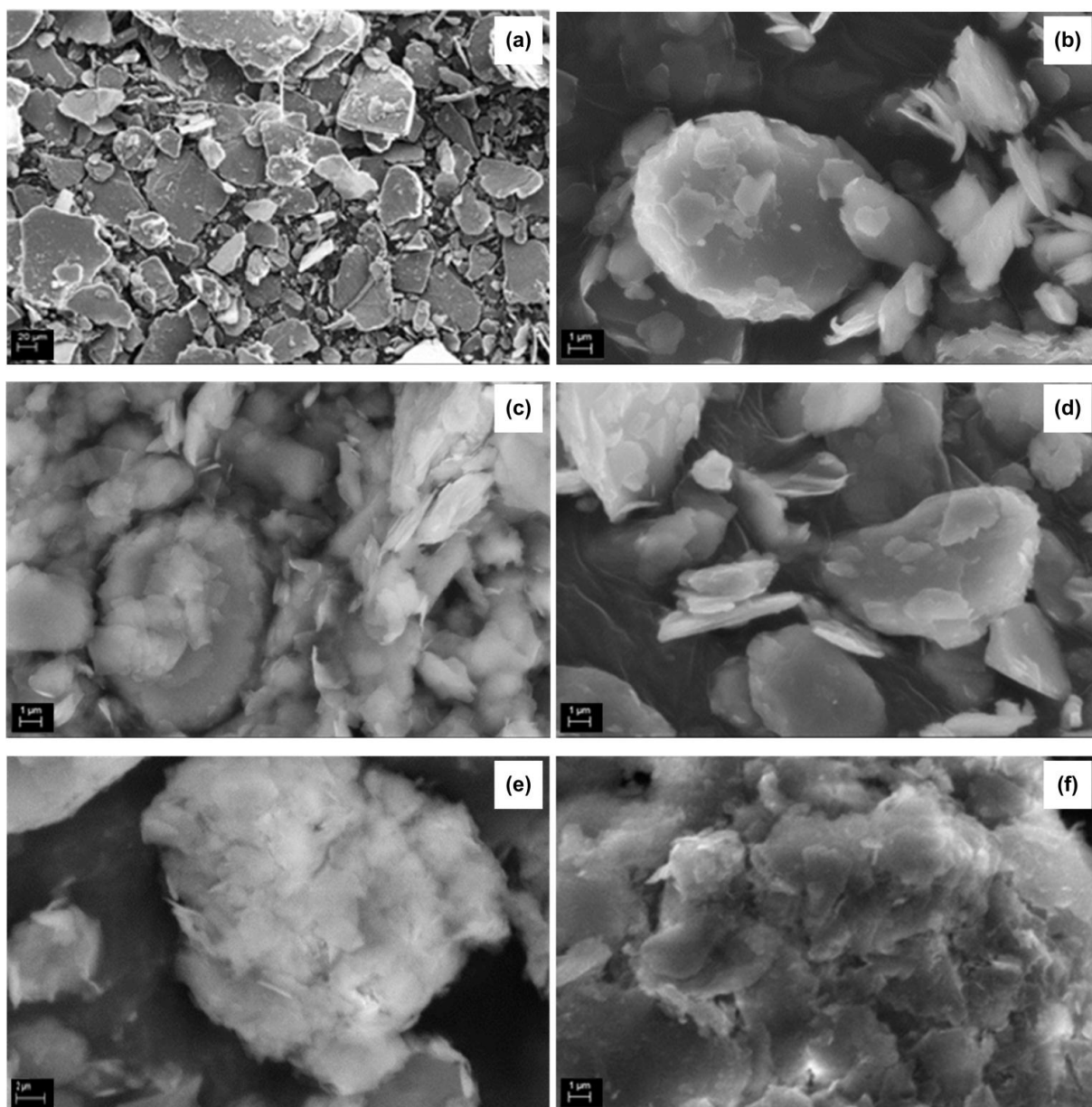


Fig. 6: Scanning Electron Micrographs of (a) Na- VMT, (b) S-V-H<sub>2</sub>O at 25°C, (c) S-V-H<sub>2</sub>O at 90°C, (d) S-V-H<sub>2</sub>O/Argon at 25°C (e) S-V-H<sub>2</sub>O<sub>2</sub> at 25°C and (f) S-V-Toluene at 25°C.

Table 1: Comparison of the elemental analysis and the atomic % of exchangeable cations of K-VMT and Na-VMT raw and sonicated samples in water and hydrogen peroxide.

Samples	%	%	%	%	%	%	%	%	Atomic % of exchangeable cations		
									SiO <sub>2</sub>	Al <sub>2</sub> O <sub>3</sub>	Fe <sub>2</sub> O <sub>3</sub>
<b>K-VMT<sup>+</sup></b>	39.78	12.61	6.52	24.12	0.89	1.07	5.92	1.45	9	71	20
<b>K-VMT sonicated 5h in H<sub>2</sub>O<sub>2</sub><sup>+</sup></b>	37.52	12.05	5.98	22.93	0.95	0.61	4.91	1.89	12	74	14
<b>Na-VMT</b>	39.08	12.25	6.16	23.82	0.11	3.25	4.07	1.13	1	45	54
<b>S-V- H<sub>2</sub>O- 25°C-5h</b>	38.09	11.69	5.95	22.73	0.19	2.88	4.16	2.25	2	48	50
<b>S-V- H<sub>2</sub>O- 90°C-5h</b>	37.98	11.79	5.37	23.10	0.37	2.33	4.62	1.20	4	55	42
<b>S-V- H<sub>2</sub>O- Argon-5h</b>	37.22	11.68	5.76	22.62	0.18	2.86	4.21	2.71	2	48	50

<sup>+</sup> Samples from reference [19] (Nguyen et al)

Table 2: BET specific surface area measured as a function of sonication time and temperature

Sample name	Na-VMT	S-V-H <sub>2</sub> O-25°C-1h	S-V-H <sub>2</sub> O-25°C-3h	S-V-H <sub>2</sub> O-25°C-5h	S-V-Tolu-25°C-5h	S-V-Argon-25°C-5h	S-V-H <sub>2</sub> O <sub>2</sub> -25°C-5h	S-V-H <sub>2</sub> O-90°C-5h	S-V-H <sub>2</sub> O-25°C-8h
BET Surface Area (m <sup>2</sup> /g)	3.6	15.4	27.8	30.9	7.7	29.2	25	31.5	34.3